Intrinsic valence and conduction bands of Si(111)-1×1

Y. He, S. Bouzidi, B.-Y. Han, L.-M. Yu, P. A. Thiry, and R. Caudano
Laboratoire Interdisciplinaire de Spectroscopie Electronique and Laboratoire de Spectroscopie Moléculaire de Surface, Institute for Studies in Interface Sciences, Facultés Universitaires Notre-Dame de la Paix, 61, rue de Bruxelles, B-5000 Namur, Belgium

J.-M. Debever
Groupe de Physique des Etats Condensés, Université de la Méditerranée, 163, avenue de Luminy, Case 901, F-13288 Marseille Cedex 9, France

(Received 6 March 1996; revised manuscript received 8 August 1996)

The valence bands of the unreconstructed H-Si(111)-1×1 are investigated using angle-resolved ultraviolet photoelectron spectroscopy. The high quality of the surface and the absence of reconstruction allow us to observe bulk bands comparable to theoretical calculations. The asymmetric dispersion of the valence bands along the $\bar{M}'\ \bar{\Gamma}\ \bar{M}$ direction of the surface Brillouin zone confirms the asymmetry observed for the conduction bands. Such an asymmetry, stemming from the fact that the family of (112) planes are not mirror planes in the bulk of Si, provides a supplementary means of disentangling bulk states from surface states. [S0163-1829(96)10848-1]

INTRODUCTION

During the past three decades many attempts have been made in order to reveal electronic and structural properties of Si(111), with relative success. While the theoretical investigations were successful,[1,2] experimental work progressed with some difficulty. This is partly due to the long delay in developing adequate tools, but it is mainly due to the complexity of the surface itself. Like most surfaces of so-called ''covalent'' semiconductors, Si(111) reconstructs itself in order to lower the high surface energy associated with the half-filled sp orbitals (dangling bonds) resulting from broken covalent bonds. The most stable Si(111) surface arrangement is the 2×1 reconstruction obtained readily by cleavage in ultrahigh vacuum (UHV), and described by the π-bonded chain model consisting of dimers in a zigzag configuration; another arrangement is the 7×7 reconstruction obtained after annealing at high temperature (around 900 °C). Some authors reported the observation of several intermediate reconstructions such as Si(111)-$\sqrt{3}\times\sqrt{3}R30°$ (Refs. 3 and 4) represented by adatoms[3] or by a lack[4] of silicon atoms; like the 7×7, the 5×5 reconstruction is accounted by the DAS model which affects four atomic layers under the surface plane with adatoms, dimers, holes, and stacking faults.[5,6]

On all these surfaces, the crystallographic diamond structure of the bulk is not preserved, and in order to examine the electronic bulk structure of silicon through its (111) surface, it is thus necessary to avoid surface reconstructions. Much effort has been made to passivate and stabilize the 1×1 ideal structure using several methods, e.g., by dosing, in UHV, the cleaved Si(111)-2×1 reconstruction or the annealed Si(111)-7×7 reconstruction by atomic hydrogen. However, this treatment does not eliminate the structural disorder of the surface and underlying layers. The only adsorbed system which gives rise to the (1×1) surface structure is the As:Si(111),[7] where every surface silicon atom is replaced by arsenic. There is an outward relaxation of 0.17 Å of the arsenic layer with respect to the initial position of the silicon atoms.[8] In that case, the first layer formed by the arsenic atoms is not inert; it exerts a negative potential on the electrons, lowering their band energy, and modifying their dispersion.[9]

Another kind of treatment consists of a wet chemical etching in a hydrofluoric acid solution in order to saturate the dangling bonds with hydrogen atoms. For a long time, this method has encountered some difficulty in obtaining long-range unreconstructed areas. Recently, Higashi *et al.*[10] succeeded in improving the procedure by selecting a proper pH value of the HF solution, thus achieving atomically flat monohydride-terminated surfaces. The high quality of such a surface is confirmed by several techniques, such as infrared reflection-absorption spectroscopy and high-resolution electron-energy-loss spectroscopy, indicating the absence of the dihydride or trihydride species.[10–12] Scanning tunneling microscopy (STM) images confirm the crystallographic 1×1 structure, while the STM spectroscopy measurements prove the absence of electronic states in the band gap, as predicted by the theory.[13] The H-Si(111)-1×1 system provides a transparent bulklike surface layer which favors the detection of bulk electronic structures due to the lack of any interaction or screening effect. Recently the occupied surface states were determined by Hricovini *et al.*[14] using synchrotron radiation, but they gave no indication concerning the bulk valence bands.

In this paper, by measuring H/Si(111), we report on the valence-band dispersion of the bulk and hydrogen-induced surface structures, investigated by angle-resolved ultraviolet photoelectron spectroscopy (ARUPS). k-resolved inverse photoelectron spectroscopy (KRIPES) results on empty conduction-band states[15] will be recalled here and added to the original ARUPS results in order to propose a complete description of the electronic structure of Si(111). The paper is organized as follows: we start by presenting the surface preparation procedure and some brief ARUPS details. Then our results are compared with theoretical predictions and previous experiments. Finally some intrinsic characteristics are revealed.

H-Si(111)-1×1 surface preparation and experimental details

The samples were cut in a *n*-type doped silicon wafer (~10 Ω cm). First, the substrates are cleaned from organic contaminants in hot trichloroethylene, and then at room temperature in acetone and in methyl alcohol. This step is followed by the removal of inorganic contaminants (trace metals and chemisorbed ions) in $NH_4OH:H_2O_2:H_2O$ (1:1:4) at 80 °C for 10 min. A brief etch in a buffered HF solution is applied before immersion in $HCl:H_2O_2:H_2O$(1:1:4) at 80 °C for 10 min; besides the cleaning role of this solution, this permits the growth of a clean oxide film. Such a film can prevent further contamination of the silicon surface before the final etching. The final step consists of oxide removal in an ammonium fluoride solution (40% NH_4F, pH=7.8) for 6 min. The principle of the final step was reported by Trucks *et al.*[16] The H-F molecule attacks the polar Si-OH bonds, leading to the formation of a highly polar Si-F species which polarizes the Si-Si backbond. Consequently, the backbond is readily attacked by HF, leaving H-Si bonds behind on the surface. Some residual physisorbed complexes such as SiF_4, NH_4OH, and HF should be removed by a final rinse. It is emphasized that it is necessary to rinse the sample in pure deionized water (18.2 MΩ cm) between each step, but it is highly desirable that the duration of the last rinse after the final etching step should be as short as possible (<10 s) in order to avoid any reoxidation. Despite the high degree of passivation of such surfaces in deionized water and in air, special caution is required when introducing the sample in UHV. An inert environment is desired, while the sample is quickly clamped on a molybdenum sample holder and attached to a transfer system in a well prebaked introduction chamber. This chamber is first pumped down slowly to 10^{-2} Torr through a leak valve in order to avoid turbulences, and then the pumping is accelerated using a turbomolecular pump. Then the sample is transferred into the UHV analysis chamber. In order to avoid any contamination or surface degradation, all hot filaments are turned off during transfer and subsequent analysis. The base pressure in the analysis chamber is 10^{-10} Torr. The chamber is equipped with low-energy electron diffraction (LEED) and x-ray photoelectron spectroscopy.

The ARUPS data are collected with an ESCA-300 electron analyzer (Scienta) (ESCA is electron spectroscopy for chemical analysis) and an ultraviolet light source (He I, Leybold-Heraeus) of 21.2-eV energy. The electron analyzer and the UV light source are installed in a fixed position and optically focused onto the sample surface. A correct focus was found by reaching both maximum intensity and minimum widths of the peaks for each polar angle. The angle-resolved measurements are performed by rotating the sample plane toward the axis of the analyzer along the two azimuthal directions.

The half-acceptance angle of the lens system of our analyzer is 8°. We emphasize that in the ESCA-300, the acceptance angle of the hemispherical analyzer is not defined by pure geometrical considerations of the entrance slit of the lens and by its distance from the sample, but rather by the entrance slit of the analyzer (0.2 mm in our present analysis configuration). However, due to an assembly defect, the magnetic shieldings of the lens and of the analyzer are not connected in our system, so that an estimation of the analyzer acceptance from electron ray tracing calculations is not reliable. This notwithstanding, we can be confident in the validity of our data because they reproduce exactly the dispersion already measured previously by other authors for the surface states. From this comparison, we can estimate the acceptance angle of our analyzer as between 2° and 3°. Unpolarized UV light is used, so that we do not need to consider polarization effects due to geometric changes when rotating the sample. A pass energy of 10 eV was used in the analyzer with an overall energy resolution of ~150 meV. The Fermi-level position was calibrated by measuring a thick Ag film.

RESULTS AND DISCUSSION

Before presenting the results, some indices need to be defined in order to clarify the data. The angular measurements were carried out on either side of the surface normal, along a given crystallographic orientation. It has been arbitrarily chosen to let $\bar{\Gamma}\bar{M}$ ($\bar{\Gamma}\bar{K}$) correspond to positive electron emission angles and $\bar{\Gamma}\bar{M}'$ ($\bar{\Gamma}\bar{K}'$) to negative angles as indicated on the figures. The combination of LEED and *Laue* patterns permits us to associate the [110] axis with $\bar{\Gamma}\bar{K}$ ([$\bar{1}$10] to $\bar{\Gamma}\bar{K}'$), and the [1 $\bar{1}$2] axis to $\bar{\Gamma}\bar{M}$ ([112] to $\bar{\Gamma}\bar{M}'$).

The ARUPS spectra measured on the H-Si(111)-1×1 surface along the $\bar{K}'\bar{\Gamma}\bar{K}$ and $\bar{M}'\bar{\Gamma}\bar{M}$ directions are presented in Figs. 1 and 2, respectively. For completeness and comparison, the right panels of each figure show the corresponding KRIPES spectra as a function of electron incidence angle.[15] All energies refer to the Fermi level. Vertical bars, in both series, indicate characteristic features determined automatically by a Gaussian fitting procedure.

The energy dispersions of these structures are displayed in Fig. 3 as a function of $k_{\parallel}$, the electron wave-vector component parallel to the surface. The valence (conduction) bands are denoted by Latin (Greek) symbols. The principal characteristics of these band dispersions is the global symmetry with respect to the surface Brillouin-zone (SBZ) center, and also the symmetry in shape and intensity of each spectra pair recorded at opposite angles along $\bar{K}'\bar{\Gamma}\bar{K}$ [Figs. 3(a) and Fig. 1]. The situation is completely different for the data measured along the $\bar{M}'\bar{\Gamma}\bar{M}$ direction [Figs. 3(b) and 2]. While some bands, such as the a' and b bands, are symmetric, others present a clear asymmetric behavior in dispersion, and are also asymmetric in some features in the spectra taken at opposite angles. Note the appearance of the E band which is clearly resolved only on one side ($\bar{\Gamma}\bar{M}'$).

It was theoretically reported by Schlüter and Cohen[1] that the ideally bare Si(111)-1×1 surface exhibits a pure surface state around the Fermi level. It is a mixture of bonding and antibonding states arising from the sp dangling-bond orbital. In the case of the H-Si(111)-1×1 system, the dangling bonds are saturated with hydrogen atoms. The hydrogen permits the formation of a nonpolarized H-Si covalent bond; thus there is no reason to expect the existence of empty surface states. By virtue of the same argument, pure valence surface states should not be found due to the absence of lone pair electrons. H-Si(111)-1×1 is nonmetallic, and its gap is free of surface states; however, it could exhibit a surfacelike state originat-

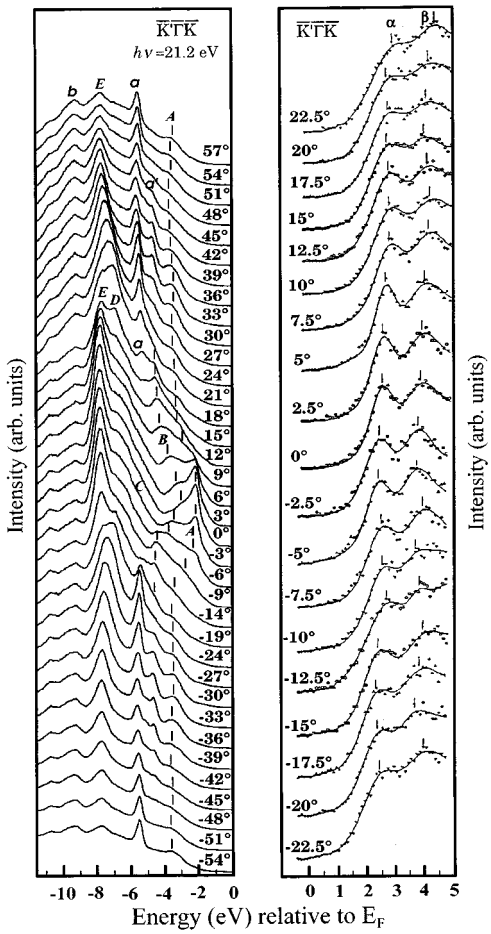

FIG. 1. ARUPS (left panel, measured with an unpolarized 21.2-eV light source) and KRIPES (right panel) spectra recorded on the H/Si(111)-1×1 surface along $K'\ \Gamma\ K$in the 1×1 SBZ. a, a', and b are surface states, A, B, C, D, and E are bulk states, α and β represent empty conduction bands.

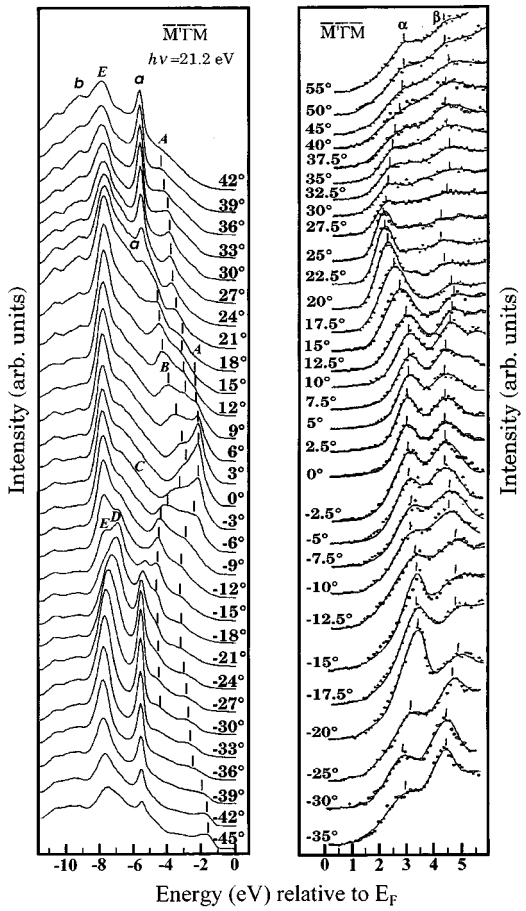

FIG. 2. ARUPS (left panel, measured with an unpolarized 21.2-eV light source) and KRIPES (right panel) spectra recorded on the H/Si(111)-1×1 surface for the $M'\ \Gamma\ M$in the 1×1 SBZ. a' and b are the surface states, A, B, C, D, and E are bulk states. α and β represent empty conduction bands.

ing from the Si-Si backbonds with a weak contribution from an H-Si bond.[1] This state has to be localized in pseudoenergy gaps. Our experimental feature a should be attributed to this state. Although these secondary band gaps are easily determined, and projected on the valence bands, their projection traces on the conduction bands are too small to be represented, which makes it difficult to identify resonant conduction surface states in the experimental data.

The theoretical prediction of the electronic structures for both valence and conduction bands of the H-Si(111)-1×1 has been significantly improved by the GW approach,[14] which is exhibited in Fig. 4. The energy scale refers to the maximum of the valence band. In our valence-band results, the two outstanding features a' and a, previously measured by Hricovini *et al.*, and identified as occupied surface states,[14] are in good agreement with the GW calculation. The polarization of these surface states has been recently investigated by synchrotron radiation induced UPS and a bulk resonance, centered at the K point of the SBZ has been shown.[17] A structure b in energy corresponds to a surface state located at about -8.4 eV which refers to the top of the valence band in the GW method. The calculation shows a very weak dispersion of this structure around $\overline{K}$, except that, while our ARUPS spectra demonstrate a flat dispersion throughout the whole 1×1 SBZ in both azimuthal directions, the feature is weak and broad along $M'\ \Gamma\ M$.

Concerning the conduction states, two features, denoted α and β, are observed outside the forbidden zone (at 2.6 and 4.0 eV above the Fermi level, respectively). They appear in the full SBZ along $M'\ \Gamma\ M$, but only along half of $K'\ \Gamma\ K$(Fig. 4). The feature α is a resonance state. Its lower branch disperses at the edge of the bulk conduction bands. It has been identified by Schlüter and Cohen[1] and Nardelli *et al.*[18] as a Si s-like state present in all calculated configurations, clean Si(111)-1×1, H-Si(111)-1×1, and Cl-Si(111)1×1, confirms its intrinsic character to silicon, and that it is not induced by hydrogen; it is a bulklike state.[1] Moreover, these two states are in good agreement with those at 2.4 and 4.0 eV, denoted L_1^c, and L_3^c, respectively, shown in the results obtained by Straub, Ley, and Himpsel,[19] on cleaved Si(111)-2×1.

In the valence bands, the A and B structures were well established as direct bulk transitions from the two uppermost valence bands to a free-electron-like final band.[20] They were

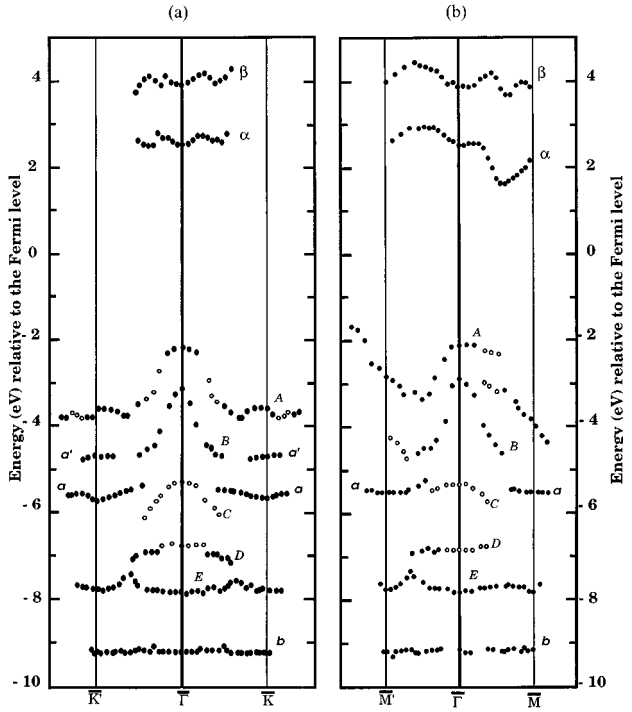

FIG. 3. Energy dispersion of conduction and valence bands of Si(111) vs $k_{\|}$, (a) along $\bar{K}'\,\bar{\Gamma}\,\bar{K}$ and (b) along $\bar{M}'\,\bar{\Gamma}\,\bar{M}$. The energy scale refers to the Fermi level.

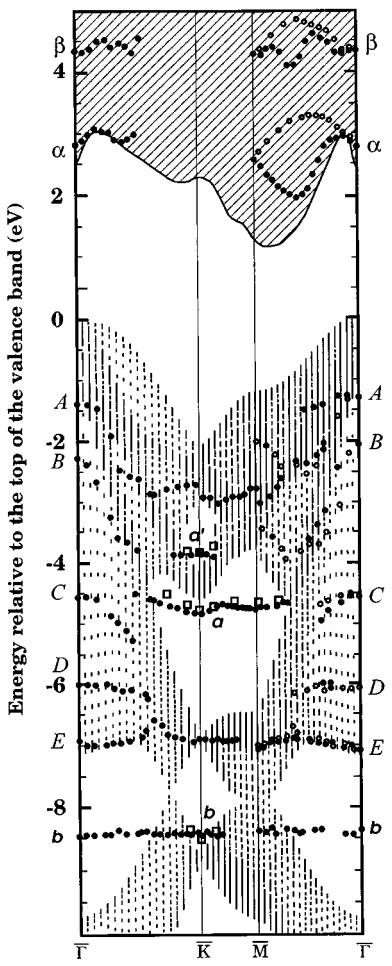

FIG. 4. The GW calculation (Ref. 14) for conduction and valence bands along $\bar{\Gamma}\,\bar{K}\,\bar{M}\,\bar{\Gamma}$ with ARUPS and KRIPES experimental data. The energies in eV are referred to the top of the valence band. The open squares represent the GW calculated surface states. The hatched area is the projection of the Si bulk GW band structure, on the (111) plane. The experimental points are represented by solid circles for the states probed along $\bar{\Gamma}\,\bar{K}$ and $\bar{\Gamma}\,\bar{M}$ and open circles for the states along $\bar{\Gamma}\,\bar{M}$.

observed on the reconstructed Si(111)-2×1 surface probed with polarized light of different photon energies of 10.2, 13.0, 15.0, and 17.0 eV,[20,21] and also on the reconstructed 7×7 surface probed with unpolarized light of 21.2-eV photon energy.[22] In our spectra, the structure B appears as a shoulder of the structure A at the $\bar{\Gamma}$ point. When dispersing, it becomes a resolvable peak. Nevertheless it disappears when the H-induced surface state (**a**) appears. As illustrated by the dependence of $\mathbf{E}(k_{\|})$ in Fig. 3(b), the asymmetric character is always observed along $\bar{M}'\bar{\Gamma}\bar{M}$ in both valence and conduction bands. For instance, note that in the lower feature (α) of the conduction bands, there is at least 1.0-eV difference between the two band branches (see Fig. 2 at $+20°$ and $-20°$). It is an interesting comparison to note that the valence feature A in the valence bands located at -2.2 eV at $\bar{\Gamma}$ also shows a comparable asymmetry of about 1.0 eV.

It has been suggested that the feature at ~7.8 eV below E_F, denoted E, is caused by a direct bulk emission from the bottom of the second valence band to a free-electron-like final state.[23] The assignment is confirmed by its location along the edge of the projection of the GW valence bands (Fig. 4).

In our ARUPS spectra, a broad hump is observed around the $\bar{\Gamma}$ point. It is deconvoluted into two components located at -5.5 and -7 eV relative to the E_F level, denoted C and D, respectively, as shown in Fig. 5, which illustrates the curve-fitting procedure used throughout this work. In contrast to core-level peaks, the line shapes and background of valence-band structures are not well established, so that one has to make reasonable and coherent assumptions: (1) We use a simple linear background because there are no physical reasons to introduce a more complicated one. (2) All peak line shapes are Gaussian, taking account of the fact that the analyzer transmission function dominates the measurements of valence-band structures. (3) The number of different peaks used for the fitting is determined by eye from the observation of ''visible'' structures, and additional peaks are kept as few as possible. (4) The widths of the peaks are allowed to vary from peak to peak, but the width is kept constant for the same peak, over a complete series of angle-resolved spectra.

Peaks C and D correspond to two bands in the slab calculation by Nardelli *et al.*[18] shown in Fig. 6 based on a surface linear muffin-tin orbitals (SLMTO) formalism in the atomic spheres approximation. Such a surface calculation produces energy bands in the two-dimensional SBZ that can be directly compared to the experiment, and that accumulate in the region of the projection of bulk bands that is repre-

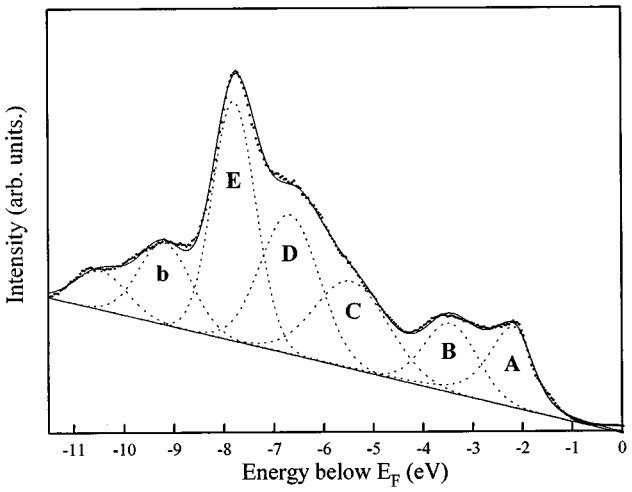

FIG. 5. The dotted line is the UPS spectrum of the H/Si(111) recorded along $\bar{\Gamma}\bar{K}'$ with a 6° emission angle. The full curve is the fitted result. The structures *A*, *B*, *C*, *D*, *E* and *b* are indicated by dashed curves. A linear background and Gaussian line shapes are used.

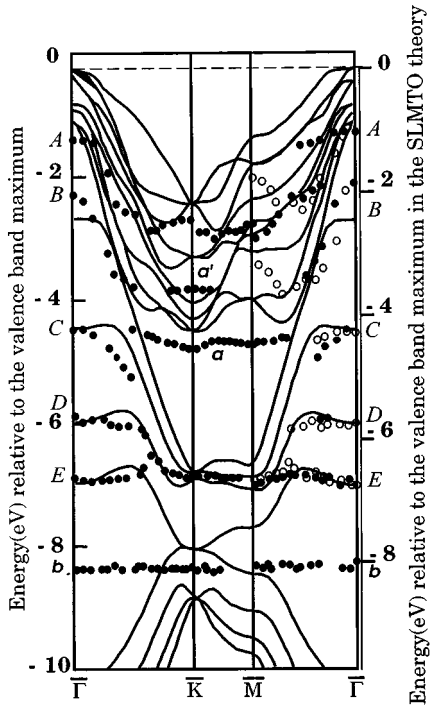

FIG. 6. The SLMTO calculation (Ref. 18) and ARUPS experimental data (this work) for valence bands. The energies in eV refer to the top of the valence band. The left and right scales are the *GW* and SLMTO references, respectively. The full curves represent the calculated bands. The experimental points are represented by solid circles for the states probed along ΓK and ΓM, and open circles for the states along ΓM.

sented by the hatched areas in Fig. 4. Interestingly, it is found in the left panel of Fig. 1 that the structure *D* becomes intense and is resolved around 20° symmetrically along both ΓK and ΓK. However, a similar symmetry is not observed along the $M'\ \Gamma\ M$ direction in the left panel of Fig. 2, where the resolved peak *D* appears on one side of Γ but is not seen on the other side. To our knowledge this is the first time that this peak has been observed either on a chemically prepared or an adsorbed H/Si(11) surface. It is found that the features *C*, *D*, and *E* fit, in a reasonable manner, the theoretical curves[18] with a 0.22-eV upward global energy shift of our data (Fig. 6). Also, the experimental bands *A* and *B* are distributed within upper dense bands, and follow the trend of the calculated curves. The main characteristic features of the H/Si(111) surface at the critical points are listed in Table I with some available theoretical data. We note the absence of states in the primary band gap as was confirmed by STM spectroscopy.[13]

It should be emphasized that an important characteristic in our ARUPS and KRIPES spectra is the asymmetry of electronic state distribution in the $M'\ \Gamma\ M$ orientation. This physical picture has been predicted by the calculated $\mathbf{E}(k_{\|})$ dispersions for the two bulk states *A* and *B* of the valence

TABLE I. Energies of conduction- and valence-band states at $\bar{\Gamma}$, $\bar{K}$, and $\bar{M}$ (in eV with respect to the top of the valence band).

Structures \ Critical points	Experiment			Theory								
				GW			SLMTO			EPP		
	$\bar{\Gamma}$	$\bar{K}$	$\bar{M}$	$\bar{\Gamma}$	$\bar{K}$	$\bar{M}$	$\bar{\Gamma}$	$\bar{K}$	$\bar{M}$	$\bar{\Gamma}$	$\bar{K}$	$\bar{M}$
α	2.8		2.6									
β	4.4		4.5									
a		−4.9	−4.8		−4.8	−4.7						
a'		−3.9			−3.9							
b		−8.4	−8.4		−8.5							
A	−1.4	−2.7	−2.8							−1.4	−2.5	−3.2
B	−2.3									−1.4	−4.8	−3.2
C	−4.5						−4.3	−6.5	−6.5			
D	−6.0	−7.0	−7.0				−5.7	−6.7	−6.8			
E	−7.0			−7.1			−6.9	−7.8	−7.4			

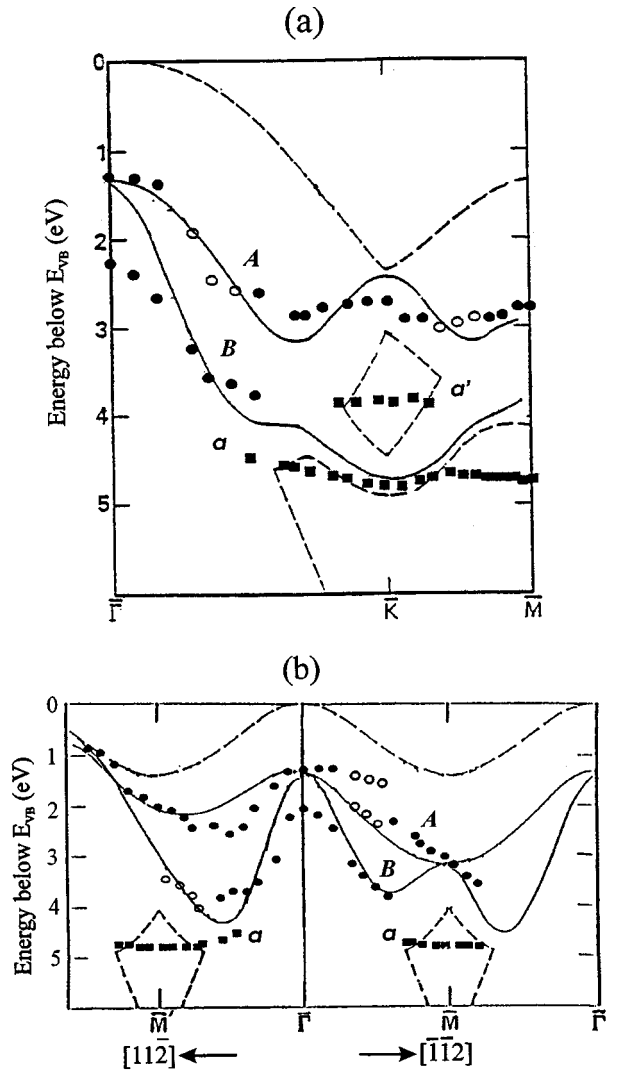

FIG. 7. Energy vs $k_{\parallel}$ relation for different azimuths (a) for $M'\ \Gamma\ M$, and (b) for $\Gamma\ K\ M$. Solid curves represent the calculated dispersions for the structures, A and B. Circles represent the experimental data (solid circles: stronger features; open circles: weaker features). Solid squares are the surface states a and a'. Dashed curves show the edge of the projected bulk band.

bands of Si(111), of which peak A shows clear asymmetry along the $M'\ \Gamma\ M$ azimuthal direction.[24] The calculated dispersions were obtained by using initial bands from an empirical pseudopotential (EPP) calculation and a free-electron parabola as the final-state band with 21.2-eV photon excitation (Fig. 7).[24] The ARUPS investigations of the Si(111)-7×7 surface, with 21.2-eV photons, showed that although the agreement between the experimental and calculated dispersions was mostly good, asymmetry along $M'\ \Gamma\ M$ was not observed.[22] The structure A (which corresponds to structure C in Ref. 22) was only detected on one side of the Γ point (along [21 1], while it was absent on the other side (along [112]). For the unreconstructed H-Si(111)-1×1 surface, not only are the experimental dispersions in good overall agreement with the calculation (Fig. 7), which is particularly true for structure A along $\Gamma \rightarrow K \rightarrow M$ [Fig. 7(a)], but also remarkable asymmetric dispersion for the structure A is demonstrated along $\bar{M}'\ \bar{\Gamma}\ \bar{M}$ [Fig. 7(b)], in keeping with the theoretical curves. Both direct and inverse photoemission data completely confirm the existence of asymmetry in the electronic structure of the H-Si(111)-1×1 surface. Therefore it can be seen that a perfectly ordered H-terminated surface is identified by symmetric and asymmetric distributions of its bulk electronic states along two major azimuths, respectively, in the SBZ.

The dispersion of structure B does not directly display any convincing asymmetry, but an asymmetry is implied through several weaker features in the [112] direction, represented by open circles in Fig. 7(b), implying the asymmetry of this structure. It is, however, noted from both Figs. 7(a) and 7(b) that the dispersion of structure B is interrupted at $k_{\parallel} \approx 0.5-0.6$ Å^{-1} relative to Γ, where the H-induced surface states of a and/or a' appear with a close initial energy. The appearance of the surface states stops the dispersion of the B state. Thus it is deduced that the structure would continue its dispersion after the $k_{\parallel} \sim 0.6$ Å^{-1}, and show asymmetry as predicted by the calculation if the structure was not affected by the surface states. This deduction is supported by the fact that the surface state a' disperses almost along the calculated bulk band of B in the vicinity of K shown in Fig. 7(a). This indicates that the two-dimensional adsorbate-induced wave function forms a linear combination with three-dimensional bulk states, thereby altering the bulk wave function and partially leading to a resonance with the bulk.[25] A comparison can be made with the As:Si(111)-1×1 surface, where the dispersion of the structure B has better agreement with the calculations, especially along $\Gamma\ K\ M$ because of the absence of a surface state nearby. However, dispersion of the structure A in the case of the As:Si(111)-1×1 is not very consistent with the calculation, due to the presence of a surface state just above it, which does not disperse along the [112] direction.[24] The observation may be interpreted as the effect of resonance between surface and bulk states.

The electronic band asymmetry originates from the crystallographic arrangement of underlying silicon layers (at least four layers). Unlike the apparent sixfold symmetry of the LEED pattern characterizing the arrangement of surface atoms, the bulk crystallographic structure has only a threefold axis. The three planes (110), (10$\bar{1}$), and (011) normal to the surface and containing the $M'\ \Gamma\ M$ azimuths are mirror planes for the $K'\ \Gamma\ K$ directions, and as a direct consequence the electronic structures along these latter directions are symmetric. Along $\bar{M}'\ \bar{\Gamma}\ \bar{M}$ [1 $\bar{1}$2], the situation is completely different, because the normal planes (112), (121), and (211), containing the $K'\ \Gamma\ K$ directions, are no longer mirror planes, and, thus, the contribution of the electronic states arising from opposite azimuthal directions is different.

CONCLUSION

The electronic structure of the silicon valence and conduction bands was completely investigated through the (111) surface, by using a chemically prepared, perfectly monohydride-passivated Si(111) surface. The investigation was done along two main characteristic azimuths of the 1×1 SBZ. The experimental dispersion of the valence bands was compared with three theoretical calculations: GW, SLMTO,

and EPP. (1) The dispersion of the surface states a, a', and b, predicted by the GW formalism, is fairly well reproduced; (2) The dispersion of bands C and D are observed in keeping with the SLMTO calculation; (3) The asymmetry of the A band, predicted by the EPP calculation along $M'\,\Gamma\,M$ is one of the most striking results of our study, as it testifies to the high perfection of the surface, and gives a strong argument in favor of the bulk nature of this state.

ACKNOWLEDGMENTS

This paper presents results obtained in the framework of the Belgian national program of Interuniversity Research Projects (PAI/IUA) on ''Sciences of Interfacial and Mesoscopic Structures'' and ''Materials Characterization'' sponsored by the Belgian Prime Minister's Office (Federal Services for Scientific, Technical and Cultural Affairs). The GPEC is Unité de Recherches Associée au CNRS No. 783.

[1] M. Schlüter and M. L. Cohen, Phys. Rev. B **17**, 716 (1978).
[2] K. C. Pandey and J. C. Philips, Phys. Rev. Lett. **32**, 1433 (1974).
[3] J. E. Northrup, J. Ihm, and M. L. Cohen, Phys. Rev. Lett. **47**, 1910 (1981).
[4] W. C. Fan, A. Ignatiev, H. Huang, and S. Y. Tong, Phys. Rev. Lett. **62**, 1516 (1989).
[5] K. Takayanagi, Surf. Sci. **164**, 367 (1985).
[6] K. Takayanagi and Y. Tanishiro, Phys. Rev. B **34**, 1034 (1986).
[7] R. S. Becker, B. S. Swartzentruber, J. S. Vickers, and M. S. Hybertsen, Phys. Rev. Lett. **60**, 116 (1988).
[8] J. R. Patel, J. A. Golovchenko, P. E. Freeland, and H.-J. Gossmann, Phys. Rev. B **36**, 7715 (1987).
[9] S. Bouzidi, T. Angot, F. Coletti, J.-M. Debever, J.-L. Guyaux, and P. A. Thiry, Phys. Rev. B **49**, 16 539 (1994).
[10] G. S. Higashi, Y. J. Chabal, G. W. Trucks, and K. Raghavachari, Appl. Phys. Lett. **56**, 656 (1990).
[11] P. Dumas and Y. J. Chabal, Chem. Phys. Lett. **181**, 537 (1991).
[12] Yan He, P. A. Thiry, Li-Ming Yu, and R. Caudano, Surf. Sci. **331-333**, 441 (1995).
[13] R. S. Becker, G. S. Higashi, Y. J. Chabal, and A. J. Becker, Phys. Rev. Lett. **65**, 1917 (1990).
[14] K. Hricovini, R. Günther, P. Thiry, A. Taleb-Ibrahimi, G. Indlekofer, J. E. Bonnet, P. Dumas, Y. Petroff, X. Blase, Xuejun Zhu, Steven G. Louie, Y. J. Chabal, and P. A. Thiry, Phys. Rev. Lett. **70**, 1992 (1993).
[15] S. Bouzidi, F. Coletti, J.-M. Debever, P. A. Thiry, P. Dumas, and Y. J. Chabal, Phys. Rev. B **45**, 1187 (1992).
[16] G. W. Trucks, K. Raghavachari, G. S. Higashi, and Y. J. Chabal, Phys. Rev. Lett. **65**, 504 (1990).
[17] J. Avila, R. Günther, M. C. Asensio, A. Taleb-Ibrahimi, and P. Dumas (private communication).
[18] M. B. Nardelli, F. Finocchi, M. Palummo, R. Di Felice, C. M. Bertoni, F. Bernardini, and S. Ossicini, Surf. Sci. **269/270**, 879 (1992).
[19] D. Straub, L. Ley, and F. J. Himpsel, Phys. Rev. Lett. **54**, 142 (1985).
[20] R. I. G. Uhrberg, G. V. Hansson, U. O. Karlsson, J.-M. Nicholls, P. E. S. Persson, S. A. Flodström, R. Engelhardt, and E.-E. Koch, Phys. Rev. Lett. **52**, 2265 (1984).
[21] R. I. G. Uhrberg, G. V. Hansson, U. O. Karlsson, J. M. Nicholls, P. E. S. Persson, S. A. Flodström, R. Engelhardt, and E.-E. Koch, Phys. Rev. B **31**, 3795 (1985).
[22] R. I. G. Uhrberg, G. V. Hansson, J. M. Nicholls, P. E. S. Persson, and S. A. Flodström, Phys. Rev. B **31**, 3805 (1985).
[23] C. J. Karlsson, E. Landemark, L. S. O. Johansson, U. O. Karlsson, and R. I. G. Uhrberg, Phys. Rev. B **41**, 1521 (1990).
[24] R. I. G. Uhrberg, R. D. Bringans, M. A. Olmstead, R. Z. Bachrach, and J. E. Northrup, Phys. Rev. B **35**, 3945 (1987); see also R. D. Bringans, R. I. G. Uhrberg, and R. Z. Bachrach, *ibid.* **34**, 2373 (1986).
[25] F. J. Himpsel, Adv. Phys. **32**, 1 (1983).